Anion Control of Voltage Sensing by the Motor Protein Prestin in Outer Hair Cells

Volodymyr Rybalchenko*[†] and Joseph Santos-Sacchi*[‡§]

*Department of Surgery (Otolaryngology),Yale University School of Medicine, New Haven Connecticut; [†]Department of Pharmacology and Neuroscience, University of North Texas Health Science Center, Fort Worth, Texas; and [‡]Department of Neurobiology and [§]Department of Cellular and Molecular Physiology, Yale University School of Medicine, New Haven Connecticut

ABSTRACT   The outer hair cell from Corti's organ possesses voltage-dependent intramembranous molecular motors evolved from the SLC26 anion transporter family. The motor, identified as prestin (SLC26a5), is responsible for electromotility of outer hair cells and mammalian cochlear amplification, a process that heightens our auditory responsiveness. Here, we describe experiments designed to evaluate the effects of anions on the motor's voltage-sensor charge movement, focusing on prestin's voltage-dependent Boltzmann characteristics. We find that the nature of the anion, including species, valence, and structure, regulates characteristics of the charge movement, signifying that anions play a more complicated role than simple voltage sensing in cochlear amplification.

INTRODUCTION

The mammalian cochlea possesses unique cellular structures evolutionarily designed for active amplification, providing enhanced detection and discrimination of acoustic frequencies beyond 70 kHz (1,2). Despite much progress, our understanding of the molecular mechanisms responsible for this active amplification within the organ of Corti remains incomplete. Nevertheless, there is a growing consensus that it is the electrically evoked mechanical activity of the outer hair cells (OHCs) that boosts auditory performance (3–6). These OHCs possess a fast electromotility arising from the recently cloned voltage-sensitive protein prestin (SLC26a5) (7,8), which is densely expressed in the OHC lateral membrane (9,10). The electrical signature of conformational changes in prestin is a displacement current or nonlinear capacitance (NLC) (11–13). The estimated millions of motor molecules (14,15) that reside within each OHC power plasma membrane surface area fluctuations (16–18), thereby predominantly producing longitudinal movements of the cylindrically shaped cells on a submillisecond timescale.

The discovery of a fundamental role for intracellular anions (Cl^- in particular) in promoting prestin's voltage sensitivity (19) gave rise to a model in which anions serve as extrinsic voltage sensors whose intramembrane movement directly alters the conformational state of prestin. The model, which we refer to as the partial anion transporter (PAT) model, is encapsulated by an animated cartoon (www.sciencemag.org/content/vol 292/ issue5525/images/data/2340/DC1/Prestin_movie.mov). It purports that the voltage-driven movement of a bound anion from the intracellular aspect of prestin toward the extracellular

aspect (resulting from a truncated transport cycle) gates prestin from the contracted to the expanded state. Thus, apparent gating charge (z) would derive from the distance (d) that the anion/ sensor charge ($q =$ ion valence $\times\ e$) moves perpendicular to the membrane field; that is, two-state Boltzmann fits of gating charge or NLC would provide an apparent gating charge of $z = d \times q$. Thus, in this model, z is expected to scale with either d or anion valence. However, the model (19) posits only monovalent anion sensors.

This initial observation was complimented by our recent observations that certain intracellular anions, which were initially considered, according to the PAT model (19), to be unable to serve as prestin's voltage sensor (e.g., SO_4^{2-}), can support NLC and shift prestin's voltage operational range (V_{op}, defined in Methods) (20). These observations led to a model for prestin voltage sensing in which anions allosterically modulate the voltage-sensing activity of intrinsic charged residues. In this model, apparent z is still obtained from fits to a two-state Boltzmann function, but it describes, instead, an equivalent charge, q, the sum of an unknown number of partial charges, through a trajectory perpendicular to the membrane field. In this model, z does not necessarily scale with anion valence. We also found that anions pass through a lateral membrane conductance, under the control of membrane stretch and voltage (20). These findings led to a hypothesis that prestin state transitions can occur at constant membrane potential (V_m), being driven by anion flux resulting from acoustically evoked OHC lateral membrane deformations (3,4,20,21). These conformational transitions would primarily result from binding and unbinding of anions, a process that could be unencumbered by the OHC's membrane RC filter (22,23). Here, we expand on our initial observation that intracellular anions significantly shift prestin's V_{op}, and we provide further data that the nature of the anion, including species, valence, and structure, regulates Boltzmann characteristics of the charge movement, indicating a more compli-

cated picture of anion interactions with prestin than a simple extrinsic voltage sensor model (19) can yield.

METHODS

Adult guinea pigs were euthanized with a halothane inhalation overdose protocol approved by the Yale University animal use and care committee. OHCs were freshly isolated from the organ of Corti after enzymatic (dispase 0.5 mg/ml) and mechanical treatment in Ca^{2+}-free medium. Cells of approximately the same size (50–70 μm) were used. Electrical recordings from voltage-clamped OHCs were done at room temperature, as described in our previous work (20). Combined leakage-free liquid bridges (Ag-ACl-TrisCl-TrisMalate-agar) were used in grounding and patch pipette circuits to minimize liquid junction potentials that were kept within ± 4 mV while Cl^--free and Cl^--containing solutions were exchanged during the experiment. These values were obtained in control test conditions with solution exchanges around an open pipette. The solution buildup within the bridge was not observed during the relatively short time of the exposure ($\sim$2–5 min) of one particular solution. The solutions were either low-Ca^{2+} or Ca^{2+}-free and K^+-free (listed in Table 1) to prevent OHC K^+ and Ca^{2+} currents. At the ion concentrations listed, the osmolarity for extracellular solutions was $\sim$325 mOsm, whereas solutions 5 mOsm lower were used intracellularly to prevent OHC swelling and effects of altered membrane tension on prestin's functional parameters (24–26). The pH of solutions was adjusted to $\sim$7.25–7.30 with TrisOH. No difference in osmolarity for equimolar solutions of short- and long-tail sulfonic anions was noticed, indicating that no micelles were formed by any of the alkyl-sulfonates tested. All chemicals were from Sigma (St. Louis, MO) and Fluka (Buchs, Switzerland).

Extracellular solutions were locally applied to the individual cells by Y tube while a bath was continuously perfused with Tris-Hepes$_{(o)}$ solution. When evaluating the effects of extracellularly applied anions on the intracellular aspect of prestin (see Figs. 3 and 4), at least a 2-min interval was allowed from the moment of extracellular solution application to the time the membrane capacitance was recorded, to allow the extracellular anions to permeate the membrane and equilibrate with the intracellular solution. Where appropriate, as noted in the text, the patch pipette solutions were exchanged during continuous recording from the cell, using the intrapipette perfusion system 2PK+ (ALA Scientific Instruments, Westbury, NY). In most experiments, 200 μM streptomycin + 400 μM acetazolamide (OHC stereocilia channels and hemichannel blockers) were added to all extracellular solutions to rule out possible influence on the data from unaccounted currents.

OHC membrane capacitance measurements

The OHC voltage-dependent membrane capacitance (C_m), i.e., the capacitance-voltage (C-V) plot, was measured by applying a command voltage protocol (ramp + superimposed two-sine (10 mV peak at 390.6 and 781.2 Hz) from holding potential $V_{hold} = 0$ mV) that allowed us to sample at 2.56 ms resolution. Subsequently, off-line extraction of C-V plots was performed using a fast-Fourier-transform-based admittance analysis (27,28) incorporated into jClamp software (SciSoft, Branford, CT).

Prestin molecular parameters

Experimentally measured OHC C-V plots were fitted with the function $C_m = C_{lin} + C_v$, where C_{lin} is the voltage-independent (linear surface area component) capacitance of the lipid bilayer, and $C_v = dQ_{nonL}/dV$ is the voltage-dependent component of C_m originating from prestin's intramembrane voltage-sensor translocation evoked by external voltage, described with a two-state Boltzmann function, $Q = Q_{max}/(1 + \exp(-ze(V - V_{pkCm})/k_BT))$. The total nonlinear fitting function for C_m (13), $C_m = C_{ln} + \{Q_{max}ze/k_BT\} \times \exp(-ze(V - V_{pkCm})/k_BT)/(1 + \exp(-ze(V - V_{pkCm})/k_BT))^2$ represents a bell-shaped C-V plot (Fig. 1, *middle*) from which the parameters of Q_{max}, z, V_{pkCm}, and C_{ln} were obtained using a nonlinear curve-fitting procedure. Q_{max} is the total charge translocated if all active prestin molecules underwent conformational transition to the alternative state. $Q_{max} = q \times N$, where q is

TABLE 1   Composition of intracellular and extracellular solutions

Solution name	Special notes	MgSO$_4$	Mg(OH)$_2$	EGTA	Malate	TrisOH	HCl
Tris-Mal$_{(i)}$	Malate^{2-}, 115	—	2	2	—	$\sim$260	—
Tris-Cl$_{(i)}$	—	2	2	$\sim$180	—	150	
Tris $-$ Mal$_{(i)}^{10Cl}$	Malate^{2-}, 107	—	2	2	—	$\sim$245	10
Tris-Hepes$_{(i)}$*	Hepes$^{(-)}$, 190	2	—	10	—	$\sim$120	—
Tris-SO$_{4(i)}$	SO$_4^{2-}$, 110; Hepes$^{(-)}$, 10	2	—	10	—	$\sim$265	—
Na-SO$_{4(i)}$	Na$_2$SO$_4$, 110; Hepes$^{(-)}$, 30	2	—	10	—	—	—
Na-PnSO$_{3(i)}$*	NaPentSO$_3$, 140; Hepes$^{(-)}$, 10	2	—	10	—	$\sim$30	
Tris-PO$_{4(i)}$	PO$_4^{3-}$, 120	—	2	10	—	$\sim$290	—
Tris-Hepes$_{(o)}$	Hepes$^{(-)}$, 210; CaSO$_4$, 0.2	5	—	—	—	$\sim$110	—
Tris-Cl$_{(o)}$	Hepes$^{(-)}$, 10; CaSO$_4$, 0.2	5	—	—	—	$\sim$155	140
Na-Cl$_{(o)}$	NaCl, 150	—	5	—	17	$\sim$26	—
Na-SO$_{4(o)}$	Na$_2$SO$_4$, 125	—	5	—	15	$\sim$21	—
Na-Mal$_{(o)}$	Na$_2$Malate, 125	—	5	—	5	$\sim$20	—
Na-MeSO$_{3(o)}$	NaMethaneSO$_3$, 150	—	5	—	13	$\sim$18	—
Na-EtSO$_{3(o)}$	NaEthaneSO$_3$, 150	—	5	—	11	$\sim$13	—
Na-PrSO$_{3(o)}$	NaPropaneSO$_3$, 150	—	5	—	12	$\sim$15	—
Na-PnSO$_{3(o)}$	Na-1-PentaneSO$_3$, 150	—	5	—	12	$\sim$15	—
Na $-$ SO$_{4(o)}^{10Cl}$	Na$_2$SO$_4$, 117; NaOH, 10	—	5	—	15	$\sim$21	10
Na $-$ Mal$_{(o)}^{10Cl}$	Na$_2$Malate, 117; NaOH, 10	—	5	—	5	$\sim$20	10
Na $-$ MeSO$_{3(o)}^{10Cl}$	NaMethaneSO$_3$, 140; NaOH, 10	—	5	—	13	$\sim$18	10
Na $-$ EtSO$_{3(o)}^{10Cl}$	NaEthaneSO$_3$, 140; NaOH, 10	—	5	—	11	$\sim$13	10
Na $-$ PrSO$_{3(o)}^{10Cl}$	NaPropaneSO$_3$, 140; NaOH, 10	—	5	—	12	$\sim$15	10
Na $-$ PnSO$_{3(o)}^{10Cl}$	Na-1-PentSO$_3$, 140; NaOH, 10	—	5	—	12	$\sim$15	10

Subscripts (i) and (o) are used to denote intracellular and extracellular solutions, respectively. All values are given in mM.
*The presence of 2 mM of $SO_{4(i)}^{2-}$ in this solution did not influence the effect of the major anion.

prestin's voltage-sensor elementary charge and N is a number of prestin molecules. The measured "apparent valence" of prestin voltage sensor (z) is defined as $z = q \times d$, where d ($0 < d < 1$) is a normalized perpendicular projection of distance traveled by the voltage sensor within the plasma membrane field (Fig. 1). V_{pkCm} is the membrane potential (V_m) at which prestin molecules are equally distributed between expanded and contracted states. It corresponds to the peak of the C_v function. Another parameter, prestin's voltage operation range, was defined as $V_{op} = \{V_{10}, V_{90}\}$, within which the probability for prestin to switch from the expanded to the contracted state varies between 10% and 90%. Within the V_{op}, prestin molecules are sensitive to V_m variations, whereas at more negative potentials the prestin population is virtually locked in the expanded state, and at more positive potentials in the contracted state. As follows trivially from the above equation for Q, the $V_{op} = V_{pkCm} \pm 2.2 k_B T/ze = V_{pkCm} \pm z^{-1} \times 56.2$ mV.

Experimental C-V curves were corrected off-line for the effects of series resistance, R_s, using a jClamp built-in algorithm. The nonlinear fitting of C-V curves was performed using the least-square algorithms incorporated in
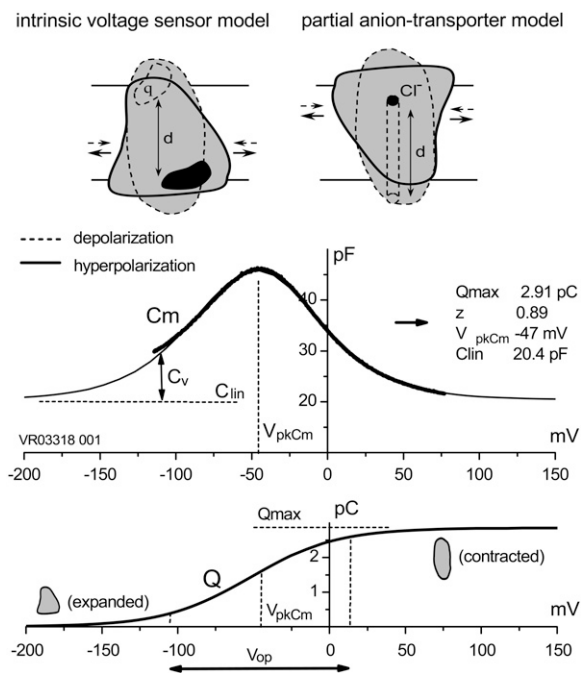

FIGURE 1 Schematic representation of the IVS and PAT models for prestin, and definitions of prestin molecular parameters. (*Upper*) Conformational transitions between prestin expanded (*solid lines*) and contracted (*dashed lines*) states after membrane hyper/depolarization cycles, result from intramembrane translocation of either 1), prestin's charged moiety q (IVS model, *left*); or 2), Cl$^-$/bicarbonate-binding moiety (PAT model, *right*). (*Middle*) Experimentally measured (in OHCs) bell-shaped C-V curve (*heavy line*) is composed of a passive capacitance of a membrane lipid bilayer (C_{lin}) and a bell-shaped voltage-dependent component of membrane capacitance (C_v) originating from intramembrane translocation of prestin's charged voltage sensor at membrane voltages within the prestin operation range (V_{op}, indicated in lower panel). The thin line is a two-state Boltzmann function first-derivative fit (see Methods) to a C-V component, from which the parameters characterizing prestin conformational transitions (Q_{max}, z, and V_{pkCm} (*inset*)) are obtained. Intracellular and extracellular solutions were Tris-Cl$_{(i)}$ and Tris-Cl$_{(o)}$, respectively. (*Lower*) Integration of the C_v component from the middle panel reproduces a Boltzmann function that characterizes prestin voltage-dependent transitions between expanded (hyperpolarization) and contracted (depolarization) states. The range of membrane potentials between 10% and 90% of prestin molecules residing in the contracted state is defined as prestin's voltage operation range (V_{op}; see Methods).
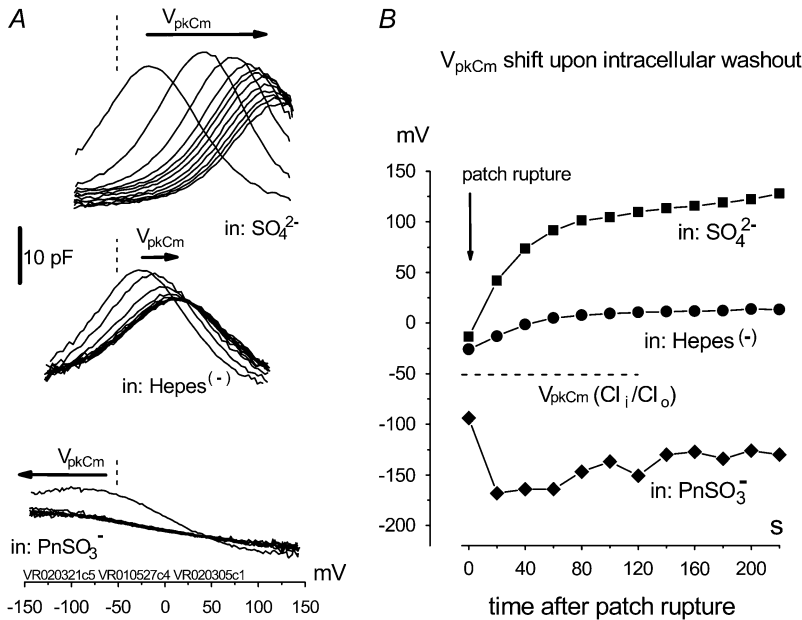
jClamp and Origin (Microcal, Northampton, MA) software ($\Delta\chi^2 < 0.05$). Data are presented as mean $\pm$ SD. The statistical significance of difference obtained for the parameters V_{pkcm}, Q_{max}, and z was calculated using one-way analysis of variance ($^{o}p < 0.1$, $^{*}p < 0.05$, $^{**}p < 0.01$, and $^{***}p < 0.001$). For Figs. 3 and 5, statistics are relative to those characteristics for Cl$^-$. For Fig. 4, statistics are for the extracellular anions (2–6) relative to those characteristics for control conditions with basal extracellular solution Na-Mal(o)10Cl (1). The number of cells tested for each anion is presented in parentheses for V_{pkcm}, and at the bottom of columns for Q_{max} and z.

RESULTS

Recently, we reported that substitution of sulfate ($SO_{4(i)}^{2-}$) for intracellular chloride ($Cl_{(i)}^-$) in guinea pig OHC cells supports NLC and shifts prestin's V_{op} to very positive membrane potentials without substantial change in electromechanical activity (20,29). We posited an intrinsic voltage sensor (IVS) model (20,29), wherein the existence of intracellular anion binding sites on prestin (binding both $Cl_{(i)}^-$ and $SO_{4(i)}^{2-}$) influences the free energy profile for prestin's voltage-dependent transitions, thereby establishing V_{op}. According to the PAT model, however, the divalent sulfate is ineffective in supporting prestin charge movement, and the positive shift in V_{op} results from decreasing chloride levels (30). Clearly, if $Cl_{(i)}^-$ removal were the sole reason for the positive V_{op} shift during the $SO_{4(i)}^{2-} \rightarrow Cl_{(i)}^-$ substitution, the shift should be in the same (positive) direction and of similar amplitude irrespective of the nature of the anion that substitutes for $Cl_{(i)}^-$. To address this issue, we monitored the changes in C-V functions during patch pipette solution washin using three different anion substitutes (SO_4^{2-}, Hepes$^{(-)}$, and 1-pentanesulfonate$^-$ (PnSO$_3^-$) (Fig. 2)). With $SO_{4(i)}^{2-}$ in the pipette, V_{pkCm} progressively shifted to high depolarizing potentials ($\sim +140$ mV) upon $Cl_{(i)}^-$ washout. The nonlinear C_v component of C-V function remained robust, in accordance with our earlier reports (20,29), but contrary to observations made on excised patches (30). With Hepes$_{(i)}^{(-)}$ anions in lieu of $Cl_{(i)}^-$, the rightward V_{pkCm} shift was less pronounced. Finally, with PnSO$_{3(i)}^-$ in the pipette, the C-V curve shift was in the opposite (negative) direction, with V_{pkCm} stabilized at extremely hyperpolarized potentials (-150 to -180 mV). The experiments depicted in Fig. 2 clearly indicate that the direction and amplitude of the shift of prestin-generated C-V functions depend on the nature of the intracellular anion and not solely on $Cl_{(i)}^-$ washout.

From our data above, it is clear that the structurally different intracellular anions SO_4^{2-}, Hepes$^{(-)}$, and PnSO$_3^-$, which can be considered sulfonate (SO_3^-)-containing anions, shift prestin's C-V function over a wide range of membrane potentials. To better understand the structure-function aspects of prestin interaction with (SO_3^-)-containing anions, we examined C-V functions of prestin in the presence of alkylsulfonic anions with increasing hydrocarbon tail lengths. Because of technical difficulties with the intrapipette exchange of multiple solutions, the four sulfonic anions: methaneSO$_3^-$ (MeSO$_3^-$), ethaneSO$_3^-$ (EtSO$_3^-$), propaneSO$_3^-$ (PrSO$_3^-$), and PnSO$_3^-$, as well as SO_4^{2-} and Cl$^-$, were consecutively applied extracellularly to the same

A

V_{pkCm}

in: SO_4^{2-}

10 pF

V_{pkCm}

in: Hepes$^{(-)}$

V_{pkCm}

in: PnSO$_3^-$

VR020321c5 VR010527c4 VR020305c1

mV

-150 -100 -50   0   50   100 150

B

V_{pkCm} shift upon intracellular washout

mV

150

patch rupture

100

50

in: SO_4^{2-}

0

in: Hepes $^{(-)}$

-50

V_{pkCm} (Cl $_i$/Cl $_o$)

-100

-150

in: PnSO$_3^-$

-200

s

0   40   80   120 160 200

time after patch rupture

FIGURE 2 Removal of $Cl_{(i)}^-$ does not determine the direction of the shift of prestin's voltage operation range. (*A*) Three different OHCs were equilibrated with $Cl_{(i)}^-$ in Tris-Cl$_{(o)}$ extracellular solution and then were voltage-clamped using patch pipettes containing intracellular Tris-SO$_{4(i)}$ (*upper*), Tris-Hepes$_{(i)}$ (*middle*), and Na-PnSO$_{3(i)}$ (*lower*) solutions. C-V curves were recorded at 20-s intervals starting at the moment of patch rupture. Upon $Cl_{(i)}^-$ substitution with intrapipette anions, the C-V characteristics exhibit a voltage shift of different amplitude and direction from $V_{pkCm}(Cl_{(i)}^-/Cl_o^-) = -51 \pm 11$ mV ($n = 9$, *dashed line*) recorded at the initial "all Cl$^-$ conditions" (Tris-Cl$_{(i)}$/Tris-Cl$_{(o)}$). The shift depends on the nature of the substitute anion and is not a result of a reduction in [Cl$^-$]$_{(i)}$. The 10 pF scale is common for all panels. The horizontal axis is the scale for V_m. (*B*) V_{pkCm} values obtained from fits (not shown) to the experimental curves for three cells from *A* were plotted against time, starting from the moment of patch rupture. The irregular time course of the $V_{pkCm}(PnSO_{3(i)}^-/Cl_o^-)$ curve is due to the difficulties in fitting C-V curves with V_{pkCm} values close to, or beyond, the limit of mechanical stability of the cell.

OHC during the experiment. In addition, we had to limit our voltage excursions to ± 100 mV to limit cell loss during the six perfusions and data collections. We have recently shown that extracellularly applied ions can pass through a nonselective OHC lateral membrane conductance (G_{metL}) to interact with prestin intracellularly (29). Intracellular malate^{2-} was used as a reference anion, since it supported the lowest Q_{max} in our previous experiments, allowing us to monitor increases in NLC due to supplemental anions. The C-V curves with fits from representative OHCs and statistics on V_{pkCm} values obtained from 10 cells ($n > 5$ for each particular anion) are presented in Fig. 3 *A*. In symmetric Mal$_{(i)}$/Mal$_{(o)}$ conditions, the reference values for $V_{pkCm}(Mal_{(i)}/Mal_{(o)}) = +99 \pm 22$ mV were at very positive membrane potentials, similar to the earlier measured $V_{pkCm}(SO_4^{2-})$. With extracellular MeSO$_3^-$ and EtSO$_3^-$, V_{pkCm} was progressively shifted to more negative potentials: $V_{pkCm}(Mal_{(i)}/MeSO_{3(o)}^-) = +79 \pm 28$ mV and $V_{pkCm}(Mal_{(i)}/EtSO_{3(o)}^-) = +59 \pm 27$ mV. The appearance of the third alkyl-carbonate in the anion PrSO$_3^-$ produced a dramatic shift of V_{pkCm} to negative membrane potentials: $V_{pkCm}(Mal_{(i)}/PrSO_{3(o)}^-) = -68 \pm 54$ mV. Further elongation of the hydrocarbon chain for PnSO$_3^-$ showed only moderate additional V_{pkCm} shift to more negative potentials: $V_{pkCm}(Mal_{(i)}/PnSO_{3(o)}^-) = -97 \pm 21$ mV. The final control applications of Na-SO$_{4(o)}$ and Na-Cl$_{(o)}$ solutions produced $V_{pkCm}(Mal_{(i)}/SO_{4(o)}^{2-}) = +96 \pm 23$ mV and $V_{pkCm}(Mal_{(i)}/Cl_{(o)}^-) = +36 \pm 13$ mV, in agreement with expected values. Statistics on Q_{max} and z values obtained in this series of experiments are presented in Fig. 3, *B* and *C*. $Q_{max}(Mal_{(i)}/Mal_{(o)}) = 0.63 \pm 0.15$ pC, $Q_{max}(Mal_{(i)}/MeSO_{3(o)}^-) = 1.16 \pm 0.33$ pC, $Q_{max}(Mal_{(i)}/EtSO_{3(o)}^-) = 1.42 \pm 0.47$ pC, $Q_{max}(Mal_{(i)}/PrSO_{3(o)}^-) = 2.44 \pm 0.45$ pC, $Q_{max}(Mal_{(i)}/PnSO_{3(o)}^-) = 2.70 \pm 0.68$ pC, $Q_{max}(Mal_{(i)}/SO_{4(o)}^{2-}) =$

1.60 ± 0.35 pC, and $Q_{max}(Mal_{(i)}/Cl_{(o)}^-) = 2.59 \pm 0.73$ pC; and $z(Mal_{(i)}/Mal_{(o)}) = 0.71 \pm 10$, $z(Mal_{(i)}/MeSO_{3(o)}^-) = 0.57 \pm 0.08$, $z(Mal_{(i)}/EtSO_{3(o)}^-) = 0.51 \pm 0.08$, $z(Mal_{(i)}/PrSO_{3(o)}^-) = 0.38 \pm 0.04$, $z(Mal_{(i)}/PnSO_{3(o)}^-) = 0.30 \pm 0.05$, $z(Mal_{(i)}/SO_{4(o)}^{2-}) = 0.58 \pm 0.07$, and $z(Mal_{(i)}/Cl_{(o)}^-) = 0.75 \pm 0.07$.

It should be noted that V_{pkCm}, Q_{max}, and z values obtained in these experiments simply serve to illustrate the general effects of these anions on NLC, since the accumulated intracellular concentration of tested anions is not known. Nevertheless, the relatively high Q_{max} values obtained for all tested anions, compared to the reference $Q_{max}(Mal_{(i)}/Mal_{(o)})$ value, indicated that accumulated concentrations of test anions were sufficient to substitute for malate^{2-} on prestin's intracellular anion-binding site(s) that modulates prestin's voltage sensor function. This issue is revisited in the experiments described in Fig. 4. It should also be noted that SO$_4^{2-}$ and PnSO$_3^-$ anions shift prestin C-V curves consistently in one direction (positive and negative, respectively) regardless of their intra- or extracellular application. This observation rules out the origin of V_{op} shifts from membrane charge screening effects and/or from liquid junction potential artifacts. The same observation ruled out electrogenic transport of those anions by prestin, since V_{pkCm} would be expected to shift in opposite directions upon switching the side of the membrane where the transported anions are applied.

Since different anion species can bind to prestin regulatory anion binding sites, it might be expected that various anions would compete for binding to these sites under normal conditions. At present, intracellular $Cl_{(i)}^-$ anions are strong candidates to be the major anions regulating prestin Q_{max} and V_{op} in OHCs. To verify whether the sulfonic anions can compete with $Cl_{(i)}^-$ for prestin regulatory binding sites, we repeated the previous experiment represented in Fig. 3 in the presence of 10 mM Cl$^-$ in the intra- and extracellular solutions. The test
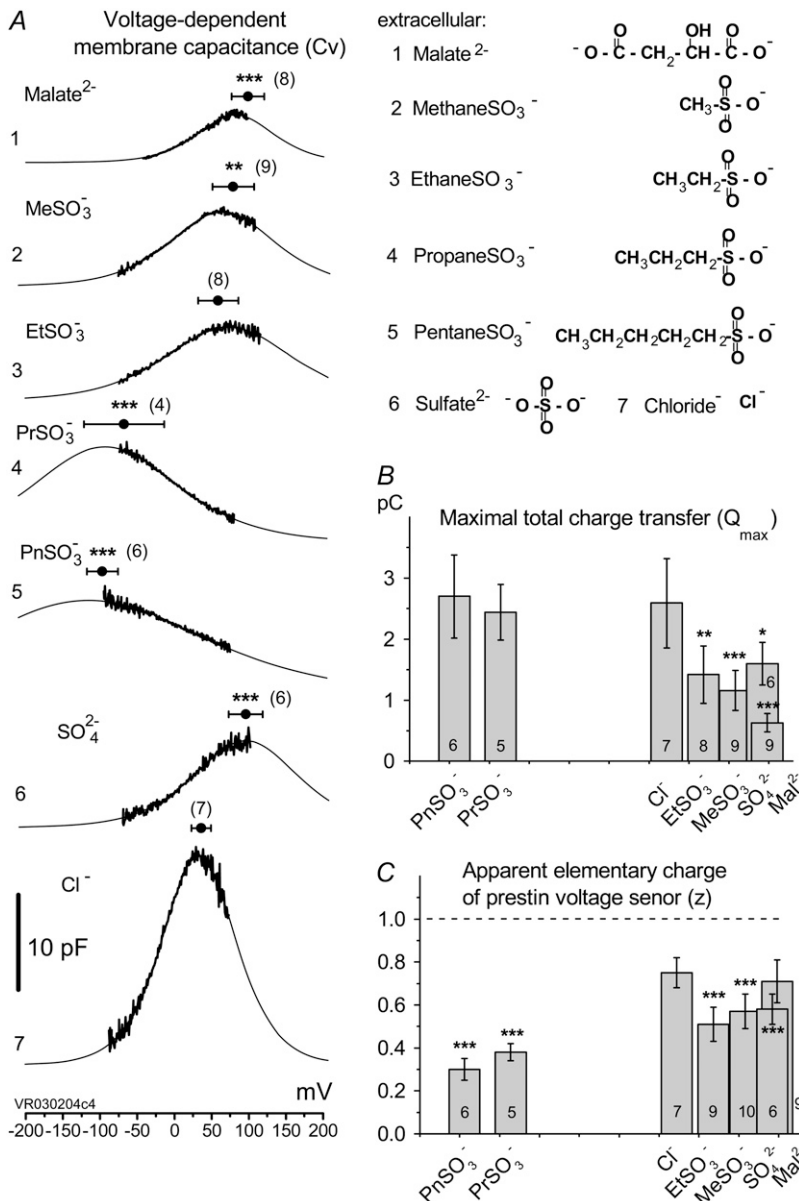
A Voltage-dependent membrane capacitance (Cv)

extracellular:

1 Malate $^{2-}$

2 MethaneSO$_3^-$

3 EthaneSO$_3^-$

4 PropaneSO$_3^-$

5 PentaneSO$_3^-$

6 Sulfate^{2-} 7 Chloride$^-$ Cl$^-$

B

C

FIGURE 3   Alkylsulfonic anions shift prestin's V_{op} over a wide range (from depolarizing to hyperpolarizing) of membrane potentials as a function of hydrocarbon chain length. (*A*) C_v-*V* curves (*thick line*) and their fits (*thin line*) obtained from the same OHC perfused with Na-Mal$_{(i)}$ intracellular solution while control anions and sulfonic anions with increasing hydrocarbon chain length were applied extracellularly in the order (of solutions) (*1*) Na-Mal$_{(o)}$, (*2*) Na-MeSO$_{3(o)}$, (*3*) Na-EtSO$_{3(o)}$, (*4*) Na-PrSO$_{3(o)}$, (*5*) Na-PnSO$_{3(o)}$, (*6*) Na-SO$_{4(o)}$, and (*7*) Na-Cl$_{(o)}$. Circles and horizontal error bars above traces represent mean ± SD for prestin V_{pkCm} values obtained in 10 cells. (*B* and *C*) Columns and vertical error bars represent statistics (mean ± SD) for Q_{max} (*B*) and *z* (*C*) values obtained from the same fits that were used to obtain V_{pkCm} parameters in *A*. Columns for the appropriate anions are placed in the order and relative position of their V_{pkCm} values on the scale of membrane potentials.

sulfonic anions were again applied extracellularly in order of their V_{pkCm} positive shift demonstrated in the previous experiment. The C-V curves and fits for representative OHCs and statistics on V_{pkCm} values obtained in five cells are presented in Fig. 4 *A*. In the present condition, where 10 mM [Cl]$_{(i)}$ is fixed, the reference value of $V_{pkCm}(\text{Mal}_{(i)}^{10Cl}/\text{Mal}_{(o)}^{10Cl}) = +2 \pm 7$ mV (Fig. 4 *A 1*) was shifted to more negative potentials than the value of $V_{pkCm}(\text{Mal}_{(i)}/\text{Cl}_{(o)}^-) = +36$ mV obtained in the previous experiment for conditions with all Cl$^-$ extracellular (Mal$_{(i)}$/Cl$_{(o)}^-$) (Figs. 3 *A 7* and 4 *A 1* (*vertical dashed line*)). The fact that the $V_{pkCm}(\text{Mal}_{(i)}/\text{Cl}_{(o)}^-)$ value is more positive than the $V_{pkCm}(\text{Mal}_{(i)}^{10Cl}/\text{Mal}_{(o)}^{10Cl})$ value indicates that the averaged accumulated [Cl$^-$]$_{(i)}$ in the previous experiment (Fig. 3) for conditions of Mal$_{(i)}$/Cl$_{(o)}^-$ was <10 mM, since lower [Cl$^-$]$_{(i)}$ would shift the prestin V_{pkCm} to more positive potentials. Thus, we estimated that accumulated intracellular sub-

plasmalemmal concentrations of sulfonic anions applied extracellularly in this and the previous experiment did not reach (and were probably significantly lower than) 10 mM.

The following values of V_{pkCm} were obtained for conditions with fixed 10 mM [Cl]$_i$ and test anions applied extracellularly (Fig. 4 *A*): $V_{pkCm}(\text{Mal}_{(i)}^{10Cl}/\text{SO}_{4\ (o)}^{2-10Cl}) = +16 \pm 6$ mV, $V_{pkCm}(\text{Mal}_{(i)}^{10Cl}/\text{MeSO}_{3\ (o)}^{-10Cl}) = +38 \pm 7$ mV, $V_{pkCm}(\text{Mal}_{(i)}^{10Cl}/\text{EtSO}_{3\ (o)}^{-10Cl}) = +31 \pm 9$ mV, $V_{pkCm}(\text{Mal}_{(i)}^{10Cl}/\text{PrSO}_{3\ (o)}^{-10Cl}) = +8 \pm 37$ mV, $V_{pkCm}(\text{Mal}_{(i)}^{10Cl}/\text{PnSO}_{3\ (o)}^{-10Cl}) = -5 \pm 27$ mV. Using the relative shift of V_{pkCm} by SO$_3$-containing anions from reference $V_{pkCm}(\text{Mal}_{(i)}^{10Cl}/\text{Mal}_{(o)}^{10Cl}) = +2$ mV as a measure of their efficacy to alter V_{op}, the following rank was obtained: MeSO$_3^-$>EtSO$_3^-$>SO$_4^{2-}$. The displacement ability by PrSO$_3^-$ and PnSO$_3^-$ could not be ranked in these experiments
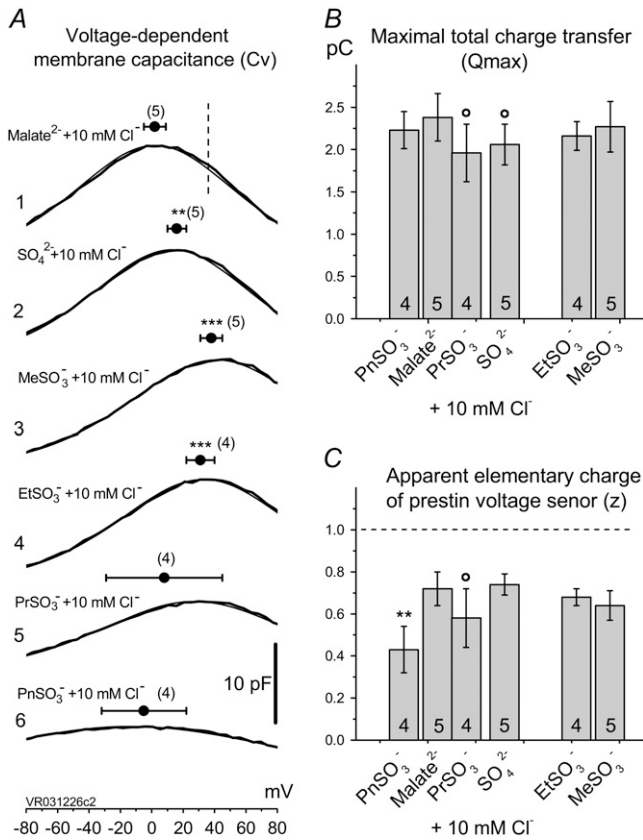
FIGURE 4 Sulfonic anions compete with Cl^- for prestin's regulatory anion-binding sites. (A) Select regions of C_v-V curves (thick lines) and their fits (thin lines, indistinguishable due to the close match) obtained from the same OHC examined at 10 mM intra- and extracellular $[Cl^-]$ "clamped" conditions with $Na - Mal_{(i)}^{10Cl}$ intracellular and reference anion and SO_3^--containing extracellular solutions applied in the order (1), $Na - Mal_{(o)}^{10Cl}$, (2), $Na - SO_{4(o)}^{10Cl}$, (3), $Na - MeSO_{3(o)}^{10Cl}$, (4), $Na - EtSO_{3(o)}^{10Cl}$, (5), $Na - PrSO_{3(o)}^{10Cl}$, and (6), $Na - PnSO_{3(o)}^{10Cl}$. Circles and horizontal error bars above traces represent mean $\pm$ SD for prestin V_{pkCm} values obtained in five cells. The vertical dashed line is drawn in the position of the $V_{pkCm}(Mal_{(i)}/Cl^-_{(o)})$ value from Fig. 3 A 7. (Note the different V_m scales in A of this figure and Fig. 3 A.) (B and C) Columns and vertical error bars represent statistics (mean $\pm$ SD) on Q_{max} (B) and z (C) values obtained from the same fits that were used to obtain V_{pkCm} parameters in A. Columns for the appropriate anions are placed in the order and relative position of their V_{pkCm} values on the scale of membrane potentials.

due to the high error margins. However, a visual inspection of C-V curves by those anions in most of the experiments (e.g., Fig. 4 A, 5 and 6) indicated their ability to modify the V_{pkCm} and z of prestin, regardless of the presence of $Cl^-_{(i)}$. This is clear from the analysis of z values obtained through this series of experiments (Fig. 4 C): $z(Mal_{(i)}^{10Cl}/Mal_{(o)}^{10Cl}) = 0.72 \pm 0.08$, $z(Mal_{(i)}^{10Cl}/SO_{4 (o)}^{2- 10Cl}) = 0.74 \pm 0.05$, $z(Mal_{(i)}^{10Cl}/MeSO_{3 (o)}^{- 10Cl}) = 0.64 \pm 0.07$, $z(Mal_{(i)}^{10Cl}/EtSO_{3 (o)}^{- 10Cl}) = 0.68 \pm 0.04$, $z(Mal_{(i)}^{10Cl}/PrSO_{3 (o)}^{- 10Cl}) = 0.58 \pm 0.14$, and $z(Mal_{(i)}^{10Cl}/PnSO_{3 (o)}^{- 10Cl}) = 0.43 \pm 0.11$. The ability of anions to decrease the parameter z (in the presence of 10 mM $[Cl^-]_{(i)}$) seemed to be stronger for long-tail anions: $PnSO_3^- > PrSO_3^- >$

$MeSO_3^- \approx EtSO_3^- > SO_4^{2-}$. The Q_{max} values in these experiments (shown in Fig. 4 B) did not vary significantly from reference conditions: $Q_{max}(Mal_{(i)}^{10Cl}/Mal_{(o)}^{10Cl}) = 2.38 \pm 0.28$ pC, $Q_{max}(Mal_{(i)}^{10Cl}/SO_{4 (o)}^{2- 10Cl}) = 2.06 \pm 0.24$ pC, $Q_{max}(Mal_{(i)}^{10Cl}/MeSO_{3 (o)}^{- 10Cl}) = 2.27 \pm 0.30$ pC, $Q_{max}(Mal_{(i)}^{10Cl}/EtSO_{3 (o)}^{- 10Cl}) = 2.16 \pm 0.17$ pC, $Q_{max}(Mal_{(i)}^{10Cl}/PrSO_{3 (o)}^{- 10Cl}) = 1.96 \pm 0.34$ pC, $Q_{max}(Mal_{(i)}^{10Cl}/PnSO_{3 (o)}^{- 10Cl}) = 2.23 \pm 0.22$ pC. For SO_4^{2-}, $MeSO_3^-$, and $EtSO_3^-$ anions with relatively low intrinsic Q_{max} (Fig. 3 B), this result might indicate an overriding control of motor function by chloride. $PrSO_3^-$ and $PnSO_3^-$ anions appear to support high Q_{max} (comparable to that for Cl^-) on their own (Fig. 3).

The series of experiments in Figs. 3 and 4 demonstrates that SO_3^--containing anions (including SO_4^{2-}) control prestin's voltage sensitivity via shifts in V_{pkCm} and alteration of the V_{op} range, or, equivalently, z. Our data can be explained by reasoning that anions applied both intracellularly and extracellularly bind to putative intracellular regulatory binding sites on prestin, thereby producing an allosteric or electrostatic influence on prestin's intrinsic voltage sensor to alter its free energy profile. There is a host of evidence that anions work on prestin intracellularly (4,19,31,32). The possibility remains that some of the alkyl anion effects on V_{op} result from the hydrophobic nature of the anions, since we and others have found that membrane lipid reactive agents can alter NLC (33–38). However, we note that in our previous experiments (32), ethanol had minimal effects below concentrations of 1%, above which V_{op} shifted to the right, in a direction opposite to the effects of ethane sulfonate. Furthermore, the inability of these alkyl anions, in the presence of 10 mM $[Cl]_{(i)}$, to shift V_{op} to the extreme voltages observed in the absence of chloride indicates that they are not working via membrane perturbation alone, but somehow are competing with chloride to establish V_{op}. Perhaps alkyl anion lipid permeability enables access to anion interaction sites of prestin not normally accessible to lipid-insoluble anions.

In its current state, the PAT model does not explain the shift of prestin's V_{op} in both negative and positive directions upon intracellular $Cl^-_{(i)}$ substitution by the various nonhalide anions (Figs. 2–4), even supposing that these anions are working as voltage-sensor substitutes.

Thus far, we have shown that anions other than Cl^- can support NLC. The capability of an alternative anion to serve as prestin's voltage sensor, as envisioned in the PAT model, can be tested knowing that the apparent valence, z, of the voltage sensor can be obtained from two-state Boltzmann function fits to C-V functions (see Methods). For di- and trivalent anions serving as voltage sensors, instead of $Cl^-_{(i)}$, the experimentally measured z parameter should double or triple relative to the values obtained with monovalent $Cl^-_{(i)}$, if the distance traveled by the replacement voltage sensor within the membrane (Fig. 1, d) remains approximately the same as for $Cl^-_{(i)}$. In Fig. 5, we present experimental C-V curves and extracted values of z and Q_{max} obtained with patch pipettes filled
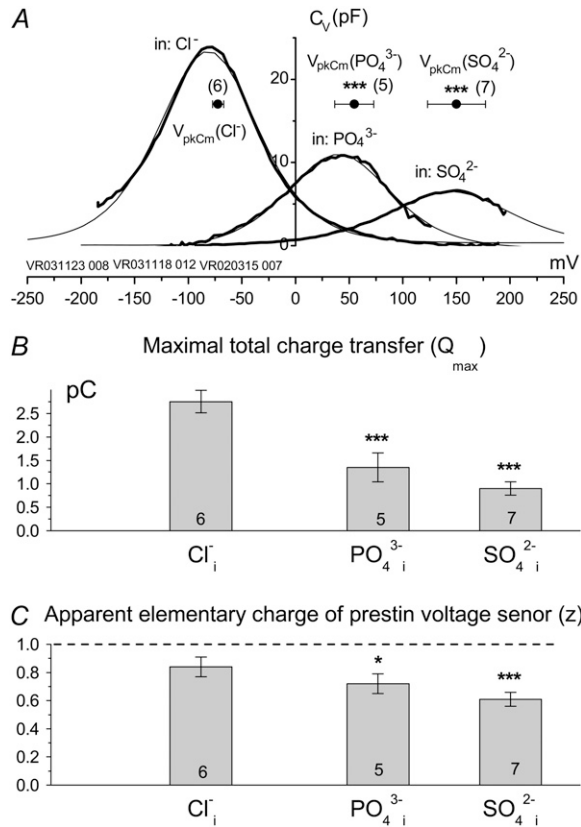
FIGURE 5 Experimentally measured apparent prestin voltage sensor elementary charge (z) is not proportional to the ionic valence of tested intracellular anions. (*A*) Voltage-dependent components (Cv) of C-V curves (*thick line*) and their theoretical fits (*thin line*) obtained from typical cells patch-clamped with pipettes filled with Tris-Cl$_{(i)}$, Tris-SO$_{4(i)}$, and Tris-PO$_{4(i)}$ solutions. The horizontal axis is the scale of membrane potentials. The solution was Tris-Hepes$_{(o)}$. Solid circles with horizontal error bars represent statistics (mean ± SD) for V_{pkCm} values obtained from fits to the C_v-V curves (see Results). (*B* and *C*) Columns and vertical error bars represent statistics (mean ± SD) for Q_{max} (*B*) and z (*C*) values obtained from the same fits that were used to obtain V_{pkCm} parameters in *A*. Columns for the appropriate anions are placed at the relative position of their V_{pkCm} values on the scale of membrane potentials.

with intracellular solutions based on monovalent Cl$^-$, and multivalent SO$_4^{2-}$ and phosphate (HPO$_4^{2-}$/PO$_4^{3-}$) anions, whereas the extracellular solution contained Cl$^-$-free Hepes$^-$-based solution. C-V curves were recorded 8–10 min after the patch rupture and cell equilibration. With Tris-Cl$_{(i)}$, the values of Q_{max}(Cl$^-$) $= 2.75 \pm 0.24$ pC and z(Cl$^-$) $= 0.84 \pm 0.07$ were obtained at V_{pkCm}(Cl$^-$) $= -72 \pm 5$ mV, resulting in prestin V_{op}(Cl$^-$) $= \{-139, -5\}$ mV ($n = 6$). With Tris-SO$_{4(i)}$, the values of Q_{max}(SO$_4^{2-}$) $= 0.90 \pm 0.14$ pC, z(SO$_4^{2-}$) $= 0.61 \pm 0.05$, and V_{pkCm}(SO$_4^{2-}$) $= +150 \pm 27$ mV resulted in V_{op}(SO$_4^{2-}$) $= \{+58, +242\}$ mV ($n = 7$). With Tris-PO$_{4(i)}$, the values of Q_{max}(HPO$_4^{2-}$/PO$_4^{3-}$) $= 1.35 \pm 0.31$ pC, z(HPO$_4^{2-}$/PO$_4^{3-}$) $= 0.72 \pm 0.07$, and V_{pkCm}(HPO$_4^{2-}$/PO$_4^{3-}$) $= +55 \pm 18$ mV resulted in $V_{op}\{$HPO$_4^{2-}$/PO$_4^{3-}\} = (-23, +133)$ mV ($n = 5$). Results obtained for z (Fig. 5 *C*) revealed that the values of z for multivalent anions decreased,

showing no correlation between the measured apparent elementary charge of prestin's voltage sensor and the ionic charge of the tested intracellular anions (Fig. 5 *C*). The observed motility of OHCs with SO$_{4(i)}^{2-}$ and HPO$_4^{2-}$/PO$_{4(i)}^{3-}$ intracellular anions remained robust, confirming the proper function of prestin's voltage sensor/effector. Reduced Q_{max} values (Fig. 5 *B*) could indicate that either the number of active prestin molecules (N) or the elementary charge of prestin's voltage sensor (q) was reduced with SO$_{4(i)}^{2-}$ and HPO$_4^{2-}$/PO$_{4(i)}^{3-}$ relative to conditions with Cl$_{(i)}^-$. The latter suggestion is more likely, given the decreased values of z. Thus, the data in Fig. 5 appear to be incompatible with the PAT model.

DISCUSSION

The prevailing concept of OHC somatic electromotility is based on voltage-dependent conformational transitions between expanded and contracted states of millions of prestin molecules residing within the lateral OHC plasma membrane. Though the primary amino acid sequence of prestin was defined several years ago (7), controversy reigns in defining prestin membrane topology (5). To sustain significant size and shape rearrangements at high frequencies (up to 70 kHz), unique thermodynamic characteristics must have evolved to set prestin close to mechanical instability, having very shallow energy minima. Therefore, conventional protein structure analysis techniques that rely on energy minima resolution could easily fail or produce ambiguous results.

An analogous controversy exists over defining the structural part of the prestin molecule that grants it voltage sensitivity. Based on an apparent disappearance of prestin voltage sensitivity and OHC electromotility upon removal of halides and other monovalent anions from the cytoplasmic side of the membrane, the initial PAT model (19) postulated that intracellular monovalent anions are prestin's extrinsic voltage sensors. The other cornerstone of the PAT model was the absence in prestin's primary sequence (relative to other SLC26 family members that lack C_v) of a clearly identifiable cluster of charged residues that might serve as prestin's voltage sensor: selective point mutations of certain scattered charged amino acids could not alter prestin's apparent unitary charge, z. An additional attraction of the PAT model was provided by an analogy with the ClC-type chloride channel model, where mixed [Cl$^-$]/voltage dependence of ClC-0 channel gating led to the suggestion that Cl$^-$ anions serve as extrinsic voltage sensors (39).

Despite a logical background, the PAT model generated some immediate concerns (40): 1), single charged-residue mutations in prestin/pendrin (SLC26a5/SLC26a6) nonconsensus regions might be an insufficient test, since voltage sensitivity of prestin might be conferred by a number of small movements of distributed partial charges rather than movement of a single point charge; and 2), nonspecific anion binding might distort the local electrostatic field influencing prestin's properties. Recent findings on ClC channel structure also preclude a direct analogy between prestin PAT and ClC

channel models by reducing the voltage-sensing role of Cl^- anions in ClC channels to a mere competition with a Glu residue carboxyl group obstructing the ClC channel's ion pore. The conformational change associated with gating of the ClC channel was limited to a small and local swing of a single amino acid side chain (41,42). Quite a different role would be expected from the Cl^- anion in the prestin PAT model: to serve as prestin's voltage sensor, it must be trapped by a cytoplasmic mobile domain to drive this domain at hyperpolarizing potentials to the extracellular side of the membrane. The mobile domain must be large enough to account for significant changes in prestin's molecular shape during conformational transitions. Specifically, simple propulsion of the Cl^- anion inside prestin would not produce significant prestin resizing due to the small atomic size of the anion itself, ~3 Å. Structural rearrangements ranging up to 8 nm^2 are estimated to occur in prestin (17,24,25,43,44).

Soon after the development of the PAT model, we provided data that prompted rethinking of the PAT model, including observations that anion substitutes cause shifts in V_{pkcm}, and that the nonhalides SO_4^{2-} and $PnSO3^-$ are capable of supporting prestin's voltage sensitivity (20). In this work, we address in depth further issues of the PAT model. First, we emphasize that shifts of prestin's V_{op} are not a function of $[Cl^-]$ per se, but are determined by the nature of alternative intracellular anions (Figs. 2–4). Indeed, the wide variation in direction and amplitude of prestin's V_{op} shift by mono- and polyvalent organic and inorganic anions does not support the idea that monovalent Cl^- and HCO_3^- are the only natural chemical modulators of prestin's voltage sensitivity. In fact, all anions tested in our experiments are capable of interacting with prestin to modify its electromotive properties. Second, we obtained statistical data demonstrating that the experimentally measured apparent valence, z, of prestin's voltage sensor does not correspond to the molecular valence of intracellular polyvalent anions, as might be expected for the PAT model (Fig. 4).

Two mechanisms could serve to reconcile this latter observation with the PAT model: 1), protonation to achieve monovalency of polyvalent anions, and 2), an inversely proportional adjustment of distance (d) traveled within the membrane field based on the size of the anion or the magnitude of the anion charge. We believe it unlikely that the relatively small differences in anion size hinder a putative hemicycle movement within the prestin core, since the anions, according to the PAT model, must drive estimated conformational changes (see above) that are orders of magnitude larger. It is also difficult to conceive how the charge magnitude (valence of the anion) could be influential in reducing the ability of the anion to pass through the membrane field. Indeed, the electrical energy to work against the load on the OHC would be amplified by the increase in valence ($E = Q \times V$), so that higher-valence anions would likely move more efficiently through the membrane for a given voltage change. Finally, although protonation during the transport cycle is conceivable, the pH effects on the motor that would be expected in such a scenario are not found (45).

The most economical explanation of our data is that although polyvalent anions support charge movement by prestin, they work not as voltage sensors but as allosteric modulators.

A conventional model would consider prestin to be a voltage-dependent protein that possesses mobile charged residues forming an IVS. Due to prestin's unique functional properties (i.e., piezoelectric operability), its voltage-dependent transitions should be accompanied by significant rearrangement of the shape of the molecule, involving movements of multiple charged amino acid residues back and forth within the membrane. Indeed, as noted above, large surface area changes in the motor have been predicted. As a result, we have considered that even intracellular charged clusters at the C-terminus of prestin might be temporarily immersed in the membrane, participating in voltage-sensing events. However, our data do not support such a role for the C-terminus charges (46). At this time, it is difficult to predict which amino acids are more and which are less important in forming the voltage sensor, because the entire molecule might contain nonuniformly distributed elements of the voltage sensor.

The discovery of prestin's Cl^- sensitivity (19) was of fundamental importance, regardless of the mechanism whereby anions influence prestin's voltage sensitivity. Indeed, we have recently shown that manipulations of Cl^- within the living animal's cochlea can drastically alter cochlear amplification in a reversible manner (4). Nevertheless, we consider the mechanism of anionic control of prestin voltage sensitivity key to understanding how the motor molecule drives cochlear amplification. In this report, we highlight two observations that are not easily reconciled with the current embodiment of the PAT model, and we reason that anions may additionally, or only allosterically, modulate prestin by binding to intracellular target sites on the protein (5,20,29). Such allosteric effects of anions have been reported before, for example, for the yeast enzyme Fet3p (47). We expect that identification of anion binding sites and of residues that contribute to prestin's apparent charge will lead to a better understanding of how this remarkable protein boosts hearing.

REFERENCES

1. Brownell, W. E., C. R. Bader, D. Bertrand, and Y. de Ribaupierre. 1985. Evoked mechanical responses of isolated cochlear outer hair cells. *Science.* 227:194–196.

2. Frank, G., W. Hemmert, and A. W. Gummer. 1999. Limiting dynamics of high-frequency electromechanical transduction of outer hair cells. *Proc. Natl. Acad. Sci. USA.* 96:4420–4425.

3. Santos-Sacchi, J. 2003. New tunes from Corti's organ: the outer hair cell boogie rules. *Curr. Opin. Neurobiol.* 13:459–468.

4. Santos-Sacchi, J., L. Song, J. Zheng, and A. L. Nuttall. 2006. Control of mammalian cochlear amplification by chloride anions. *J. Neurosci.* 26:3992–3998.

5. He, D. Z., J. Zheng, F. Kalinec, S. Kakehata, and J. Santos-Sacchi. 2006. Tuning in to the amazing outer hair cell: membrane wizardry with a twist and shout. *J. Membr. Biol.* 209:119–134.

6. Ashmore, J. 2008. Cochlear outer hair cell motility. *Physiol. Rev.* 88:173–210.

7. Zheng, J., W. Shen, D. He, K. Long, L. Madison, and P. Dallos. 2000. Prestin is the motor protein of cochlear outer hair cells. *Nature.* 405:149–155.

8. Liberman, M. C., J. Gao, D. Z. He, X. Wu, S. Jia, and J. Zuo. 2002. Prestin is required for electromotility of the outer hair cell and for the cochlear amplifier. *Nature.* 419:300–304.

9. Huang, G., and J. Santos-Sacchi. 1994. Motility voltage sensor of the outer hair cell resides within the lateral plasma membrane. *Proc. Natl. Acad. Sci. USA.* 91:12268–12272.

10. Belyantseva, I. A., H. J. Adler, R. Curi, G. I. Frolenkov, and B. Kachar. 2000. Expression and localization of prestin and the sugar transporter GLUT-5 during development of electromotility in cochlear outer hair cells. *J. Neurosci.* 20:RC116.

11. Ashmore, J. F. 1989. Transducer motor coupling in cochlear outer hair cells. *In* Mechanics of Hearing. D. Kemp and J. P. Wilson, editors. Plenum Press, New York. 107–113

12. Santos-Sacchi, J. 1990. Fast outer hair cell motility: how fast is fast? *In* The Mechanics and Biophysics of Hearing. P. Dallos, C. D. Geisler, J. W. Matthews, M. A. Ruggero, and C. R. Steele, editors. Springer-Verlag, Berlin. 69–75.

13. Santos-Sacchi, J. 1991. Reversible inhibition of voltage-dependent outer hair cell motility and capacitance. *J. Neurosci.* 11:3096–3110.

14. Huang, G., and J. Santos-Sacchi. 1993. Mapping the distribution of the outer hair cell motility voltage sensor by electrical amputation. *Biophys. J.* 65:2228–2236.

15. Gale, J. E., and J. F. Ashmore. 1997. The outer hair cell motor in membrane patches. *Pflugers Arch.* 434:267–271.

16. Kalinec, F., M. C. Holley, K. H. Iwasa, D. J. Lim, and B. Kachar. 1992. A membrane-based force generation mechanism in auditory sensory cells. *Proc. Natl. Acad. Sci. USA.* 89:8671–8675.

17. Iwasa, K. H. 1994. A membrane motor model for the fast motility of the outer hair cell. *J. Acoust. Soc. Am.* 96:2216–2224.

18. Santos-Sacchi, J., and E. Navarrete. 2002. Voltage-dependent changes in specific membrane capacitance caused by prestin, the outer hair cell lateral membrane motor. *Pflugers Arch.* 444:99–106.

19. Oliver, D., D. Z. He, N. Klocker, J. Ludwig, U. Schulte, S. Waldegger, J. P. Ruppersberg, P. Dallos, and B. Fakler. 2001. Intracellular anions as the voltage sensor of prestin, the outer hair cell motor protein. *Science.* 292:2340–2343.

20. Rybalchenko, V., and J. Santos-Sacchi. 2003. Cl$^-$ flux through a nonselective, stretch-sensitive conductance influences the outer hair cell motor of the guinea-pig. *J. Physiol.* 547:873–891.

21. Fridberger, A., and J. B. De Monvel. 2003. Sound-induced differential motion within the hearing organ. *Nat. Neurosci.* 6:446–448.

22. Santos-Sacchi, J. 1989. Asymmetry in voltage-dependent movements of isolated outer hair cells from the organ of Corti. *J. Neurosci.* 9:2954–2962.

23. Santos-Sacchi, J. 1992. On the frequency limit and phase of outer hair cell motility: effects of the membrane filter. *J. Neurosci.* 12:1906–1916.

24. Iwasa, K. H. 1993. Effect of stress on the membrane capacitance of the auditory outer hair cell. *Biophys. J.* 65:492–498.

25. Gale, J. E., and J. F. Ashmore. 1994. Charge displacement induced by rapid stretch in the basolateral membrane of the guinea-pig outer hair cell. *Proc. R. Soc. Lond. B. Biol. Sci.* 255:243–249.

26. Kakehata, S., and J. Santos-Sacchi. 1995. Membrane tension directly shifts voltage dependence of outer hair cell motility and associated gating charge. *Biophys. J.* 68:2190–2197.

27. Santos-Sacchi, J. 2004. Determination of cell capacitance using the exact empirical solution of partial differential Y/partial differential C_m and its phase angle. *Biophys. J.* 87:714–727.

28. Santos-Sacchi, J., S. Kakehata, and S. Takahashi. 1998. Effects of membrane potential on the voltage dependence of motility-related charge in outer hair cells of the guinea-pig. *J. Physiol.* 510:225–235.

29. Rybalchenko, V., and J. Santos-Sacchi. 2003. Allosteric modulation of the outer hair cell motor protein prestin by chloride. *In* Biophysics of the Cochlea: From Molecules to Models. A. Gummer, editor. World Scientific Publishing, Singapore. 116–126.

30. Fakler, B., and D. Oliver. 2003. Functional properties of prestin: how the motor molecule works. *In* Biophysics of the Cochlea: From Molecules to Models. A. Gummer, editor. World Scientific Publishing, Singapore. 110–115.

31. Kakehata, S., and J. Santos-Sacchi. 1996. Effects of salicylate and lanthanides on outer hair cell motility and associated gating charge. *J. Neurosci.* 16:4881–4889.

32. Song, L., A. Seeger, and J. Santos-Sacchi. 2005. On membrane motor activity and chloride flux in the outer hair cell: lessons learned from the environmental toxin tributyltin. *Biophys. J.* 88:2350–2362.

33. Fang, J., and K. H. Iwasa. 2007. Effects of chlorpromazine and trinitrophenol on the membrane motor of outer hair cells. *Biophys. J.* 93:1809–1817.

34. Rajagopalan, L., J. N. Greeson, A. Xia, H. Liu, A. Sturm, R. M. Raphael, A. L. Davidson, J. S. Oghalai, F. A. Pereira, and W. E. Brownell. 2007. Tuning of the outer hair cell motor by membrane cholesterol. *J. Biol. Chem.* 282:36659–36670.

35. Spector, A. A., N. Deo, K. Grosh, J. T. Ratnanather, and R. M. Raphael. 2006. Electromechanical models of the outer hair cell composite membrane. *J. Membr. Biol.* 209:135–152.

36. Santos-Sacchi, J., and M. Wu. 2004. Protein- and lipid-reactive agents alter outer hair cell lateral membrane motor charge movement. *J. Membr. Biol.* 200:83–92.

37. Brownell, W. E., A. A. Spector, R. M. Raphael, and A. S. Popel. 2001. Micro- and nanomechanics of the cochlear outer hair cell. *Annu. Rev. Biomed. Eng.* 3:169–194.

38. Raphael, R. M., A. S. Popel, and W. E. Brownell. 2000. A membrane bending model of outer hair cell electromotility. *Biophys. J.* 78:2844–2862.

39. Pusch, M., U. Ludewig, A. Rehfeldt, and T. J. Jentsch. 1995. Gating of the voltage-dependent chloride channel ClC-0 by the permeant anion. *Nature.* 373:527–531.

40. Meech, R., and M. Holley. 2001. Ion-age molecular motors. *Nat. Neurosci.* 4:771–773.

41. Dutzler, R., E. B. Campbell, and R. MacKinnon. 2003. Gating the selectivity filter in ClC chloride channels. *Science.* 300:108–112.

42. Dutzler, R., E. B. Campbell, M. Cadene, B. T. Chait, and R. MacKinnon. 2002. X-ray structure of a ClC chloride channel at 3.0 A reveals the molecular basis of anion selectivity. *Nature.* 415:287–294.

43. Adachi, M., and K. H. Iwasa. 1999. Electrically driven motor in the outer hair cell: effect of a mechanical constraint. *Proc. Natl. Acad. Sci. USA.* 96:7244–7249.

44. Santos-Sacchi, J. 1993. Harmonics of outer hair cell motility. *Biophys. J.* 65:2217–2227.

45. Tunstall, M. J., J. E. Gale, and J. F. Ashmore. 1995. Action of salicylate on membrane capacitance of outer hair cells from the guinea-pig cochlea. *J. Physiol.* 485:739–752.

46. Bai, J. P., D. Navaratnam, H. Samaranayake, and J. Santos-Sacchi. 2006. En block C-terminal charge cluster reversals in prestin (SLC26A5): effects on voltage-dependent electromechanical activity. *Neurosci. Lett.* 404:270–275.

47. Davis-Kaplan, S. R., C. C. Askwith, A. C. Bengtzen, D. Radisky, and J. Kaplan. 1998. Chloride is an allosteric effector of copper assembly for the yeast multicopper oxidase Fet3p: an unexpected role for intracellular chloride channels. *Proc. Natl. Acad. Sci. USA.* 95:13641–13645.